Competition between Intramolecular Hydrogen Bonds and Solvation in Phosphorylated Peptides: Simulations with Explicit and Implicit Solvent

Sergio E. Wong, Katarzyna Bernacki, and Matthew Jacobson*

Department of Pharmaceutical Chemistry, University of California—San Francisco, San Francisco, California 94134

Received: August 14, 2004; In Final Form: December 13, 2004

The atomic-level mechanisms of protein regulation by post-translational phosphorylation remain poorly understood, except in a few well-studied systems. Molecular mechanics simulations can in principle be used to help understand and predict the effects of protein phosphorylation, but the accuracy of the results will of course depend on the quality of the force field parameters for the phosphorylated residues as well as the quality of the solvent model. The phosphorylated residues typically carry a −2 charge at physiological pH; however, the effects of phosphorylation can sometimes be mimicked by substituting Asp or Glu for the phosphorylated residue. Here we examine the suitability of explicit and implicit solvent models for simulating phospho-serine in both the −1 and −2 charge states. Specifically, we simulate a capped phosphorylated peptide, Ace-Gly-Ser-pSer-Ser-Nme, and compare the results to each other and to experimental observables from an NMR experiment. The first major conclusion is that explicit water models (TIP3P, TIP4P and SPC/E) and a Generalized Born implicit solvent model provide reasonable agreement with the experimental observables, given appropriate partial charges for the phosphate group. The Generalized Born results, however, show greater hydrogen bonding propensity than the explicit solvent results. Distance dependent dielectric treatments perform poorly. The second major conclusion is that many ensemble-averaged properties obtained for the phosphopeptide in the −1 and −2 charge states are strikingly similar; the −1 species has a slightly higher propensity to form internal hydrogen bonds. All of the results can be rationalized by quantifying the strength of the P−O/H−N hydrogen bond, which depends on a sensitive balance between strongly favorable charge/dipole and dipole/dipole interactions and strongly unfavorable desolvation.

Introduction

Post-translational phosphorylation serves as a control mechanism in a myriad of cellular processes including metabolic pathway regulation,[1] extracellular signal transduction,[2] ion channel regulation[3,4] and cell cycle progression.[5−7] The hydroxyl groups of tyrosine, serine, and threonine are targeted for phosphorylation in eukaryotic cells whereas histidine and aspartic acid are the most frequent targets in prokaryotes.[7,8] The introduction of the phosphate ion, which predominantly carries a negative two charge at neutral pH, perturbs the electrostatic potential and quite often the conformation of the modified protein.[7] Even in absence of rearrangement, the change in electric field and the steric hindrance from a phosphate group can have biologically significant consequences, e.g., promoting or opposing protein−protein interactions.[1]

Theoretical studies can in principle be used to (1) gain insight into the physical phenomena that drive the effects of phosphorylation, and (2) predict the effects of phosphorylation on proteins where the phosphorylated structure remains unsolved. The number of such studies, although still relatively small, has been increasing rapidly over the past few years.[6,9−23] Although force field parameters for phosphorylated residues are still not well established, prior studies using phosphorylated residues have obtained partial charges and other parameters from nucleotide parameter sets,[9,24] quantum mechanical calculations[6,25] or alternative methods.[26]

This study evaluates the suitability of current solvent models for simulating phosphorylated proteins and peptides. Phosphorylated side chains typically carry a −2 charge at physiological pH, although the pK_a of the phosphate group is only ∼6, and the −1 species may be present in certain proteins or under low pH conditions. We consider both protonation states in this work, and focus primarily on two questions:

1. Are explicit and implicit solvent models suitable for treating phosphorylated residues with a −2 charge? To our knowledge, no systematic study of this type has been performed previously. The standard 20 amino acids, of course, have net charges between +1 and −1, and thus the large literature on the suitability of various solvent models for biomolecular simulations provides little direct guidance on their suitability for −2 charged phosphorylated side chains. At the simplest level, the increased magnitude of the electrostatic interactions between the charge and water dipoles suggests that species with a −2 charge may provide a more challenging test of water models, both explicit and implicit, than species with a single or no net charge. Specific deficiencies of implicit solvent models have been reported for side chain analogues with single charges,[27,28] due to inadequate treatment of first-shell solvation effects, and these types of errors might be expected to be amplified for a −2 species, for example due to dielectric saturation effects.[29] With respect to explicit solvent, different fixed charge models have shown significantly different results on systems of interacting charged species.[30] Neglect of solvent polarization could become a significant source of error when a −2 charge is simulated with a fixed-charge water model.[31] On the other hand, recent simulations on nucleic acids, using explicit[32−34] and a

10.1021/jp046333q CCC: $30.25
Published on Web 03/01/2005

Generalized Born implicit[35] solvent model, provide some grounds for optimizm about the ability of widely used solvent models to treat highly charged systems.

2. What are the differences between the −1 (protonated) and −2 (unprotonated) charge states of phosphorylated residues, in terms of their hydrogen bonding interactions in aqueous solution? We were motivated to address this question, in part, by the puzzling observation that substituting a phosphorylated residue with Asp or Glu sometimes, but not always, mimics the effects of phosphorylation. A simple hypothesis might be that Asp/Glu mimics phosphorylation only when the phosphorylated residue is predominantly in the protonated (−1) state in vivo. Alternately, the ability of Asp/Glu to mimic a phosphorylated residue might be a more subtle function of the precise environment of the residue, e.g., type and geometries of hydrogen bonding interactions formed by the phosphorylated residue. This work does not completely address this issue, but explores some surprisingly subtle differences in the hydrogen bonding interactions of phospho-serine in the −1 and −2 charge states.

As a first step toward addressing these questions, we simulate a small phosphorylated peptide, Ace-Gly-Ser-pSer-Ser-Nme, using explicit (TIP3P,[36] SPC/E[37] and TIP4P[36]) and implicit (Generalized Born-Surface Area[38,39] and a distance dependent dielectric) solvent models. We choose to study this relatively small system because (1) NMR measurements ($^3J_{NH-CH}$ coupling constants) were made on this system[40] and (2) it is computationally tractable and (3) it isolates the local effects of phosphorylation. The simulation results using the various solvent models are compared to each other and to experimental data.[40] Although NMR measurements exist for phosphotyrosine and phosphothreonine in the same short peptide model, we focused on the phosphoserine peptide because the $^3J_{NH-CH}$ ensemble averages converged much more rapidly. Previously, Brownian dynamics simulations were performed on the same peptide, but only a distance dependent dielectric (DDD) was used to incorporate solvent effects.[26] The calculated coupling constants agreed with experiment, within 0.1 Hz, for the unphosphorylated peptide simulations, but the agreement was poorer for the phosphorylated peptide. The use of a distance dependent dielectric was cited as a possible reason for disagreement with experiment. The key conclusion of our work is that, given appropriate partial charges for the phosphate group, the explicit solvent models and, perhaps more surprisingly, GB/SA implicit solvent model both produce good agreement with experiment.

In analyzing our results, we pay particular attention to the hydrogen bonding interactions of the phosphate group with backbone amide and hydroxyl groups in the peptide. These chemical groups are two of the three most common hydrogen bond partners of phosphorylated amino acids in the Protein Data Bank (PDB).[41] In our simulations, the dynamics are dominated by two states: one in which the phosphate forms no intramolecular hydrogen bonds, and one in which it forms multiple hydrogen bonds with backbone NH groups N-terminal to the phosphate group. The strength of the P−O/H−N hydrogen bond, which depends on both the partial charges and solvent model, is the critical determinant of agreement with experiment. Surprisingly, the singly and doubly charged phosphopeptide simulations show similar ensemble averages, with the overall hydrogen bonding propensity being slightly higher for the −1 species.

Methods

Molecular Dynamics Simulations. All molecular dynamics simulations in this study were performed by using the Amber 7 package[42] with the parm99 parameter file. The peptides were capped with an acetyl group (Ace) at the N-terminus and *N*-methyl amine (Nme) at the C-terminus; i.e., the sequence was Ace-Gly-Ser-pSer-Ser-Nme. Atom types for the phosphate moiety are already present in the parameter file (for the nucleic acids), therefore no new atom types were needed. We note that, although the ff99 force field is known to overstabilize helical conformations,[43] we did not observe this behavior in the phosphopeptide simulations; as will be seen below, hydrogen bond interactions of the phosphate group appear to be a dominant factor in determining the observed backbone conformations. In all simulations, a weak-coupling algorithm[44] kept the temperature and/or pressure constant. The temperature coupling constant, tcoup, for all production phase runs was 2 ps. The temperature coupling constant during equilibration was 1 ps for the implicit solvent simulations and 2 ps for the explicit solvent simulations. For all constant pressure simulations, the pressure coupling constant was 2 ps as well. Trajectory snapshots were saved every picosecond.

Explicit solvent simulations were prepared by immersing the solute in a rectangular water box with a 10 Å clearance from the box walls in every axis. In the case of TIP3P, a preequilibrated water box (WATBOX216) was employed as solvent. For TIP4P and SPC/E, the solvent molecules were placed in the box by using the "solvatebox" command in tleap (Amber module for system preparation). The initial box volume was 49968 Å^3 (37.40 Å × 42.62 Å × 31.35 Å) for all explicit solvent simulations. Sodium counterions were used to maintain electroneutrality. Periodic boundary conditions were imposed, and electrostatics were treated by using the particle mesh Ewald method,[45−47] with default parameters in Amber 7. The charge grid dimensions were 36, 40 and 27 Å and the nonbonded interaction cutoff in real space was 8 Å. A fourth-order B-spline interpolation was employed. Before equilibration, 2000 steps of steepest descent minimization helped relax the system. The equilibration protocol was as follows: the system was heated to 300 K in 25 ps; a constant pressure and temperature equilibration phase of 100 ps followed; subsequently, the system underwent a further NVT equilibration period of 50 ps. Following these equilibration phases, a production run of at least 15 ns was performed. The production run was performed at constant temperature and volume; the integration step was 1 fs and bonds involving hydrogen were constrained by using the SHAKE algorithm.[48]

Implicit solvent simulations were performed by using the Generalized Born-Surface Area (GB/SA) model with the radii by Tsui et al.[39] GB/SA simulations were equilibrated for 100 ps. The system was heated to 300 K over 5000, 1 fs, time-steps and maintained at that temperature for the remainder of the equilibration. A production run of 40 ns followed. The integration time step was 1 fs. The simulations were run at a constant temperature of 300 K.

The simulations using distance-dependent dielectric (DDD) were performed by using a replica exchange method.[49−51] Due to the poor shielding of electrostatics in this type of simulation and the large charge on the phosphate ion, strong hydrogen bonds form, and thermal energy (at 300 K) is insufficient to break them on the time scale of the simulation. As a result, the trajectories can become trapped in local minima at room temperature. The replica exchange method was used to sample more efficiently the conformational space of the peptide. In this method, *N* replicas of the system at *N* temperatures are run simultaneously. Periodically, every 50 ps in this study, an attempt to exchange the Cartesian coordinates among the

replicas occurs, on the basis of the Metropolis criterion.[51] If an exchange attempt is successful, the momenta are rescaled such that

$$p^{\text{new}} = \sqrt{\frac{T_{\text{new}}}{T_{\text{old}}}} p^{\text{old}} \tag{1}$$

The temperatures employed in this study were 300, 321, 348, 380, 418, 465, 524, 600 and 680 K. These were chosen to maintain a ~50% exchange probability between replicas. An equilibration run of 200 ps in which no exchanges were attempted was followed by 1 ns of exchange equilibration, and finally a 20 ns production run. Only the replica at 300 K was employed for the trajectory analysis.

Statistical analysis of the trajectories was performed by following the procedure outlined by Janke.[52] The analysis consists of calculating an autocorrelation function for the observable, determining a correlation time from the correlation function, and then using the correlation time to estimate the error of the mean. The correlation function is given by

$$C(t) = \frac{\langle O_i O_{i+t} \rangle - \langle O_i \rangle^2}{\langle O_i^2 \rangle - \langle O_i \rangle^2} \tag{2}$$

where O_i represents the value of the observable O at the ith trajectory time point. The integrated autocorrelation time is

$$\tau = {}^1/_2 + \sum_{j=1}^{N} C(j)\left(1 - \frac{j}{N}\right) \tag{3}$$

where N is the total number of points in the trajectory. As t gets larger, the statistical sampling for the calculation of $C(t)$ deteriorates and the sum diverges. To avoid this problem, the sum in eq 3 is truncated once $N > 6\tau$. Finally, error of the estimator of the expectation (mean) of the observable O is

$$\epsilon = \sqrt{2\tau \frac{\sigma^2}{N}} \tag{4}$$

where σ^2 represents the variance of the observable O, and N equals 6τ. Figure S1 (Supporting Information) provides typical graphs of the backbone dihedral angle θ (the relevant angle for the coupling constant calculation) as a function of time as an additional measure of the adequacy of sampling.

Quantum Chemistry/Partial Charge Calculations. All quantum mechanical calculations were performed on ethyl phosphate with the Jaguar package[53] (Schrödinger, Inc.). The initial geometry employed had a P−O bond distance of 1.55 Å for the ester bond and 1.46 Å for the acidic oxygens. Geometry optimization of the phosphate ion was carried out at the HF/6-31G** level, incorporating a condensed phase environment via a self-consistent reaction field (SCRF) algorithm.[54,55] Single point calculations were also performed at the LMP2/cc-pvtz(-f) level, in vacuo and with a SCRF.

Calculation of Experimental Observables. NMR vicinal coupling constants were calculated by the Karplus equation[56]

$$J(\theta) = A\cos^2(\theta) + B\cos(\theta) + C \tag{5}$$

with $A = 6.51$, $B = -1.3$ and $C = 1.5$.[57] The angle θ is the dihedral angle between the amide hydrogen and the alpha carbon hydrogen in the backbone of each residue. The average coupling constant over the trajectory was calculated for comparison with experiment. We note that coupling constant data for glycine are usually not included in the fitting of the Karplus equation parameters.

Hydrogen bonds were identified by using a distance cutoff of 2.5 Å between a polar hydrogen and the hydrogen bond acceptor, and no angular cutoff. The hydrogen bond probabilities were calculated by counting the number of trajectory frames where a given hydrogen bond was formed and dividing by the total number of frames.

To define the overall polarity of the P−O bond using different partial charges, we defined a "bond dipole" by using the following expression,

$$\vec{\mu} = \sum_i \vec{R}_i \delta_i \tag{6}$$

where $\vec{\mu}$ is the dipole moment, $\vec{R}_i$ is the position vector for the ith atomic charge and δ_i is the charge at that position. We chose to set the origin at the bond midpoint. The total bond length used was 1.46 Å, and hence the value of R in eq 6 was 0.73 Å.

Clustering of Trajectories. To gain insight into the structural states visited during the simulations, the trajectories were clustered by using the MMTSB tools set.[58] The metric for hierarchical clustering was the RMSD between heavy atoms (-jclust option in cluster.pl). This software tool chooses an optimized number of clusters on the basis of the criterion by Xu and co-workders.[59] In this approach a function, E, of the minimum of between-cluster distances (MBCD) and sum-of-square error (SSE) is evaluated at every hierarchical level; the optimal level corresponds to a maximum in E. E is defined by

$$E(i) = \frac{M(i) - M(i+1)}{\sqrt{J(i)} - \sqrt{J(i+1)}} \tag{7}$$

where "i" is the partition level, $M(i)$ and $J(i)$ corresponds to the MBCD and SSE at the partition level i, respectively. The MBCD, denoted $M(i)$, is defined by

$$M(i) = \min[d_{ij}] \qquad i < j,\ i, j = 1, 2, ..., n \tag{8}$$

where d_{ij} is defined by

$$d_{jk} = \sqrt{\frac{n_j n_k}{n_j + n_k}} |m_j - m_k| \qquad j, k = 1, 2, ..., i \tag{9}$$

and n_j and m_j denote the number of members in cluster j and its mean, respectively. SSE (J), denoted $J(i)$, is defined by

$$J(i) = \sum_{k=1}^{i} J_k \tag{10}$$

where

$$J_k = \sum_{x \in X_k} ||x - m_k||^2 \tag{11}$$

In eq 11, m_k corresponds to the mean of cluster k, as previously defined.

A total of 2000−4000 structures were subjected to clustering from each trajectory (snapshots were taken at 10 ps intervals). A representative structure for each cluster was identified as the member closest to the cluster centroid.

GB/SA Single Point Energy Calculations. To study the energetics of hydrogen bonding between a phosphate group and an amide hydrogen, single point energy calculations, using GB/

TABLE 1: Several Charge Sets Proposed for a Phosphate Group[a]

geometry optimized	method	phosphorus charge	acidic oxygen charge	ester oxygen charge	P−O bond dipole (D)
no	AM1-BCC	1.371	−0.969	−0.655	8.193
yes	HF/6-31G*	1.449	−0.992	−0.665	8.546
yes	HF/cc-pvtz(-f)	1.568	−1.025	−0.669	9.079
yes	HF/cc-pvtz(-f)/LMP2/SCRF	1.495	−1.050	−0.657	8.911
no	HF/6-31G*	1.767	−1.077	−0.686	9.957
no	HF/cc-pvtz(-f)	1.778	−1.082	−0.687	10.013
no	HF/cc-pvtz(-f)/LMP2/SCRF	1.719	−1.114	−0.687	9.919
N/A	OPLS	1.920	−1.120	−0.700	10.644

[a] Abbreviations are defined in the text.

SA as a solvent model, were performed. The calculations were carried out along a collinear P−O−H−N coordinate, and used ethyl phosphate and *N*-methyl ethanamide ($CH_3C(=O)NHCH_3$) as a model system for the hydrogen bonding. In the case where the protonated phosphate moiety was examined, ethyl biphosphate was employed. The energy calculations were performed at 0.125 Å intervals for O−H distances between 1.5 and 11 Å.

Results and Discussion

In this section, results from simulations of the capped Gly-Ser-pSer-Ser peptide using several solvent models are compared with each other and with experimental backbone $^3J_{NH-CH}$ coupling constants. We first consider the choice of atomic charges of the phosphate ion and their effect on the computed observable. This analysis is performed by using the TIP3P water model, the Generalized Born-Surface Area (GB/SA) implicit solvent model, and a distance dependent dielectric treatment. We focus primarily on the −2 pSer residue, but present some results for the protonated, −1 pSer peptide for comparison.

Calculation of Atomic Charges for Phosphate Ion. We have invested considerable effort in determining atomic partial charges for the phosphate group, because interactions with the surrounding solvent and intramolecular hydrogen bonding partners depend sensitively on the particular charges assigned. Note that we do not carry out a full parametrization of the phosphorylated residue; instead, we use atom types and covalent (bond, angle, torsion) parameters defined for nucleic acids. However, because our goal is to evaluate the suitability of solvent models for simulating the phosphopeptide, we feel that it is critical to deconvolute, insofar as possible, the effect of the partial charges chosen for the phosphate group from the effect of the solvent model. Therefore, in much of the rest of the paper, we employ several different sets of partial charges for molecular dynamics simulations, providing recommendations for partial charges that we believe to be most accurate.

Here we carry out quantum mechanical calculations at several levels of theory, ranging from semiempirical to ab initio calculations with approximate treatment of configuration interaction and solvent effects. Many methodologies have been described for computing atomic charges for use in a force field description of a chemical group. The ff99AMBER force field atomic charges were originally computed using a restricted electrostatic potential (RESP)[60] fitting protocol, with HF/6-31G* quantum calculations. This level of theory overestimates dipole moments relative to experimental gas phase results, but frequently provides a good estimate of dipole moments in water. Quantum calculations that use larger basis sets and implicitly account for a condensed phase environment are now computationally tractable, and we have chosen to explore the charges produced by some of these more sophisticated ab initio calculations as well.

Atomic charges were obtained by electrostatic potential fitting.[61,62] The structure of the ethyl phosphate ion was taken from the work of Feng et al.[6] We performed calculations by using this geometry as well as a minimized structure, with the 6-31G** basis set and a self-consistent reaction field (SCRF)[54,55] representation of aqueous solvation. The highest level of theory used for obtaining partial charges was cc-pVTZ(-f)/LMP2/SCRF (i.e., correlation treated at the level of "local" Moller−Plesset second-order perturbation theory,[63] and an SCRF treatment of solvent effects). For comparison, we calculated a set of charges with the semiempirical AM1-BCC method as implemented in the Antechamber module in AMBER 7. Furthermore, we also compared our results with the charges from the OPLS force field.[64] The results are shown in Table 1.

The results in Table 1 vary significantly and depend on both the geometry and methodology. However, several conclusions can be drawn. First the OPLS force field parameters are clearly outliers and should not be used. Second, the ester oxygen charge is consistent over the set, -0.66 ± 0.03. Third, contrary to expectations, the polarization of the P−O bond is not larger for the 6-31G* results than for results with larger basis sets. Finally, among the different calculations, the relative variation in bond dipole is greater than the relative variation of charges on the individual atoms, especially the phosphorus. Specifically, the larger partial charges for the P on the nonoptimized structure seem to partially compensate for the longer bond length. We use the bond-dipole as the *x*-axis in Figure 1, which summarizes many of the key results discussed below.

Because the different methods in Table 1 yield disparate results for the phosphate atomic charges, we tested the effect of varying the atomic charges on our simulation results. In an effort to explore systematically the range of possible atomic partial charges, we chose not to test every charge set in Table 1, but to test a representative group of charge sets that spans these results, as shown in Table 2. Though not all of these charges were obtained from the quantum mechanical calculations, they are quite reasonable. One of the charge sets was directly taken from Table 1 (AM1-BCC charges) wheeas another one is nearly equal to the results from the HF/cc-pvtz(-f)/LMP2/SCRF calculation (phosphorus charge of 1.495 versus 1.50). The charge set with a phosphorus charge of 1.8 has the same dipole moment that the OPLS charges whereas the charge set with a phosphorus charge of 1.65 serves as an intermediate between the latter two. Once the phosphorus and acidic oxygen charges were chosen, the ester oxygen was adjusted slightly to maintain an integral charge value for the entire molecule. We note that the ester oxygen only rarely forms any hydrogen bonds in any of our simulations; we do not consider it further.

Dependence of Results on Atomic Charges and Solvent Model. Molecular dynamics simulations were performed by utilizing all charge sets listed in Table 2 with the TIP3P explicit water model, the Generalized Born-Surface Area (GB/SA) implicit solvent model, and distance dependent dielectric (with $\epsilon = r$ and $\epsilon = 4r$). Figure 1a,d show the calculated coupling constants as a function of P−O bond dipole moment. The Gly1

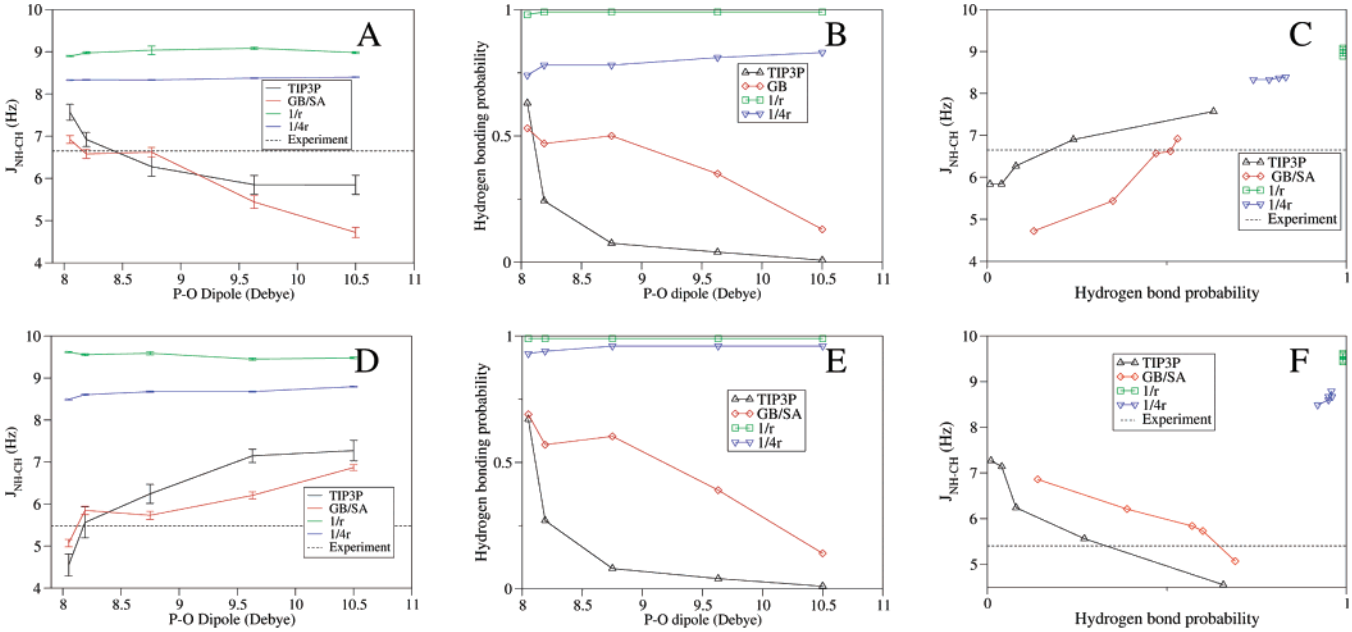

Figure 1. Phosphopeptide backbone coupling constants depend on degree of hydrogen bonding between the phosphate group and backbone amide NH groups. The P−O dipole modulates hydrogen bonding allowing a clear isolation of its effects. (A) Dependence of calculated *J* coupling constant on P−O dipole moment for Ser2. (B) Dependence of phosphate hydrogen bonding to Ser2 backbone amide on the P−O dipole moment. The larger dipole is better stabilized by solvent rather than by hydrogen bonding. (C) Calculated Ser2 *J* coupling constant as a function of hydrogen bonding probability to its backbone amide. The dependence observed in this graph links hydrogen bonding to changes in backbone conformational population differences. (D)−(F) are the corresponding graphs for pSer3.

TABLE 2: Charge Sets Used in This Study (All Charges in au)

phosphorus charge	acidic oxygen charge	P−O bond dipole (D)
1.371	−0.969	8.193
1.400	−0.900	8.053
1.500	−1.000	8.753
1.650	−1.100	9.628
1.800	−1.200	10.504

and Ser4 coupling constants are insensitive to the charge set and are not shown. [The coupling constant for Gly1 is consistently miscalculated for all the water models. This may reflect an inherent problem in the force field, problems in the interpretation of the experimental data, or the use of Karplus equation constants not explicitly parametrized for Gly.] For the central two residues, Ser2 and pSer3, the results are dramatically sensitive to the charges employed; however, the changes are systematic. The results are reassuring in the sense that agreement with experiment, within statistical error, is attainable in the range of charges tested for both explicit solvent and GB/SA.

Comparing the solvent models, one clearly sees that the distance dependent dielectric (DDD) simulation results are consistently inferior to those of the explicit solvent and GB/SA simulations (Figure 1a,d). Because this is true for all charge sets, it is not due to a poor electrostatic representation of the phosphate ion and indicates a fundamental deficiency of DDD for treating highly charged species. We note that our results, using an $\epsilon = r$ distance dependent dielectric, differ from previous results obtained with Brownian dynamics.[26] The differences probably arises from a combination of the following three factors: (1) we did not include a nonpolar surface area term in the DDD simulations, (2) the Gasteiger charges employed in the previous study are outside the range studied here (much smaller), and (3) the force fields used are different (AMBER vs CHARMM). Though the specific results are not comparable, both studies agree the DDD treatment yields poor results for the phosphopeptide with the −2 charge (much more so in our results than in the previous study). The inadequate performance of the DDD models is not surprising, given the very crude treatment of solvation afforded by DDD models.

More surprising is the similarity of the results obtained from simulations using TIP3P water and using the GB/SA model. Although the absolute coupling constants do not agree precisely, the trend as a function of P−O bond dipole is strikingly similar. This result suggests that a version of GB/SA may be appropriate for the simulation of phosphorylated systems, which would permit greatly improved computational efficiency in the case of large proteins. The best overall agreement with experiment, for TIP3P and GB/SA, occurs with P−O bond dipole of roughly 8.2−8.8. The partial charges obtained with HF/6-31G* lie in this range, and the higher level HF/cc-pvtz(-f)/LMP2/SCRF partial charges lie at the upper end of this range. On this basis, we suggest that the following partial charges for the −2 pSer/pThr group should be appropriate for most molecular mechanics simulations: +1.45 to +1.50 for the P, −0.99 to −1.05 for the acidic oxygens, and −0.66 for the ester oxygen.

In the remainder of this section, we explore the ensembles obtained by the various simulations in more detail, emphasizing the strengths of internal hydrogen bonds, which provide a compact explanation for all of the key trends we observe.

Intramolecular Hydrogen Bonding Interactions. Upon visualizing the simulations,[65] we observed that the phosphate group hydrogen bonds most commonly to the backbone amide NH groups. This type of interaction has biological relevance. In a survey of the Protein Data Bank (PDB), we have found that backbone amides are the second most frequent hydrogen bond partner, after Arg, for the phosphate groups in phosphorylated proteins (results not shown). In one common motif, the phosphate group forms multiple hydrogen bonds with amide groups at the N-terminus of a helix. To explore the role of hydrogen bonding in the dynamics, we calculated the probability of observing phosphate group hydrogen bonds in the MD trajectory. Table 4 shows the probability, for all models tested, of hydrogen bond formation between the phosphate ion and each of the backbone amide groups.

TABLE 3: Comparison of Calculated *J* Coupling Constants with the Experimental Result[a]

	TIP3P	TIP4P	SPC/E	GB/SA	DDD ($\epsilon = r$)	DDD ($\epsilon = 4r$)	experiment
Gly1	4.47 (0.03)	4.71 (0.04)	4.55 (0.03)	4.12 (0.03)	2.95 (0.01)	3.92 (0.02)	5.63 (0.12)
Ser2	6.28 (0.23)	5.99 (0.18)	6.35 (0.22)	6.62 (0.11)	9.04 (0.10)	8.33 (0.01)	6.65 (0.12)
pSer3	6.24 (0.23)	6.51 (0.28)	6.02 (0.20)	5.73 (0.10)	9.58 (0.40)	8.68 (0.02)	5.48 (0.12)
Ser4	7.72 (0.10)	7.72 (0.06)	7.84 (0.07)	7.37 (0.03)	9.26 (0.04)	8.05 (0.01)	6.93 (0.12)

[a] The error of the mean for each result is in parenthesis. For the experimental measurements, the reported error is also in parenthesis.

TABLE 4: Phosphate Group Hydrogen Bonding Probability to Peptide Backbone Amides[a]

	TIP3P	TIP4P	SPC/E	GB/SA	DDD ($\epsilon = r$)	DDD ($\epsilon = 4r$)
Gly1	6.4% (3%)	0.0% (0%)	0.7% (0.7%)	56.3% (4%)	100.0% (0.01%)	80.2% (0.5%)
Ser2	7.6% (3%)	0.2% (0.2%)	1.5% (0.7%)	50.8% (4%)	99.9% (0.02%)	78.5% (0.4%)
pSer3	8.4% (3%)	0.5% (0.3%)	2.6% (0.9%)	60.4% (4%)	100.0% (0.0005%)	95.6% (2%)
Ser4	0.1% (0.05%)	0.0% (0%)	0.1% (0.05%)	7.8% (2%)	100.0% (0.01%)	81.0% (0.6%)

[a] Each backbone amide is labeled by its residue name and number. The standard error of the mean is in parenthesis.

In general, explicit solvent simulations generate significantly lower (below 10%) hydrogen bond probabilities than the implicit treatments (mostly above 50%). The distance dependent dielectric models grossly overestimate the hydrogen bonding probability (nearly 100%).

Because intramolecular hydrogen bonding appears to play an important role in these simulations, we studied the hydrogen bonding probability as a function of the P−O dipole (Figure 1b,e). The results in Figure 1b,e may appear counterintuitive because they show that a larger dipole moment reduces the hydrogen bond probability to an amide NH group. However, this simply indicates that a larger dipole is more stable when solvated in bulk water than when forming a hydrogen bond to a backbone amide. A well organized hydration shell and bulk dielectric response stabilize the ion in water. Because hydrogen bonding disrupts both of these, it is not unreasonable that increasing the P−O dipole may destabilize hydrogen bonds. The experimental observable seems to be dominated by the equilibrium between hydrogen bonding of the phosphate ion to water versus hydrogen bonding to amide hydrogens. As the equilibrium shifts, so does the corresponding coupling constant (Figure 1c,f). Hydrogen bonding imposes a geometrical constraint on the backbone angular distribution, which is reflected in the backbone $^3J_{NH-CH}$ coupling constants. Therefore, there is a clear physical connection between the hydrogen bond probability and the angular distribution for the coupling constant calculation.

It is interesting to note that, although the explicit solvent and GB/SA simulations show similar agreement with the experimental observables, the GB/SA results show substantially greatly hydrogen bonding propensity. The explanation for this discrepancy appears to be related to a generic deficiency of implicit solvent models to reproduce certain first-shell solvation effects, specifically the "solvent-separated minima" observed in explicit solvent potentials of mean force for ion pairs and hydrogen bonds.[27,28] Figure S2 illustrates this effect for the phosphopeptide studied here. In the explicit solvent simulations, only a small population of direct hydrogen bonds between the phosphate and Ser2 amide group is observed. The direct hydrogen bonds are those with close contact between donor and acceptor, and are included in our hydrogen bond statistics, where we have used a cutoff distance of 2.5 Å. However, there is a significant population of "solvent-separated hydrogen bonds" for the explicit solvent simulations, which correspond to a distance of ~4.5 Å between donor and acceptor. This population is essentially completely absent from the GB/SA simulations, where there appear to be only 2 states, to a good approximation (direct hydrogen bond, and no hydrogen bond). It appears that the experimental observables, which reflect the ensemble of backbone conformations, are not very sensitive to the differences between direct and solvent-separated hydrogen bonds. Thus, we argue that the apparent increased "hydrogen bonding propensity" seen in the GB/SA simulations is largely a result of using a short cutoff distance which does not capture the solvent-mediated hydrogen bonds that dominate in explicit solvent.

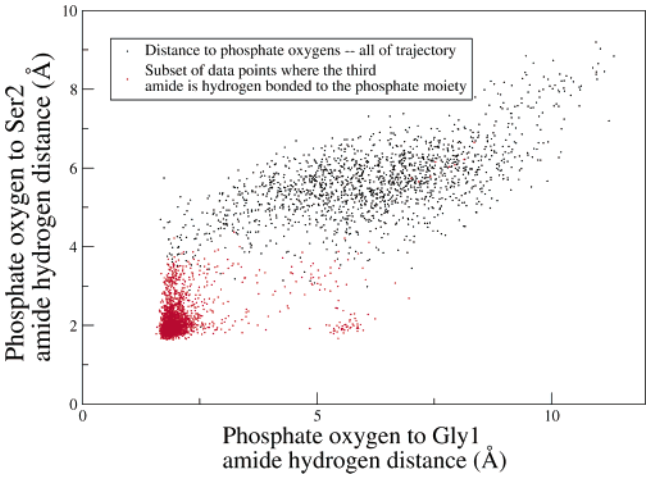

Figure 2. Cooperativity of formation of hydrogen bonds to the backbone NH groups. The axes represent the shortest distance between the phosphate acidic oxygens and the NH groups on Gly1 (*x*) and Ser2 (*y*). The points in black were calculated for all structures clustered (every 10 ps). The points in red correspond to a subset of the structures in which the phosphate group forms a hydrogen bond to the pSer3 amide group. The data shown are from the GB/SA simulation. The results for explicit solvent (TIP3P) are similar, but the density of points in the lower left corner is smaller.

We also investigated the correlation of hydrogen bond formation between the phosphate group and the various backbone amide groups, and found evidence of a cooperative transition involving the formation of multiple hydrogen bonds. Specifically, we calculated the shortest distance between the acidic phosphate oxygens and backbone amides of residues 1 and 2. These distances are plotted against each other in Figure 2. For clarity, only every tenth trajectory frame was used for this analysis. The red dots represent the subset of the structures in which the phosphate group formed a hydrogen bond to the third backbone amide. Similar graphs were obtained for both GB/SA and explicit solvent and we show only the GB/SA results. It is clear that phosphate hydrogen bonding to the amide group on pSer3 strongly increases the probability of hydrogen bonding to both the first and second residue. The hydrogen bonding probability for amides 1 and 2, once the hydrogen bond to amide 3 is formed, ranges from 50 to 70% (much larger than the product of individual probabilities). The probability of forming a hydrogen bond increases by up to 10-fold when a

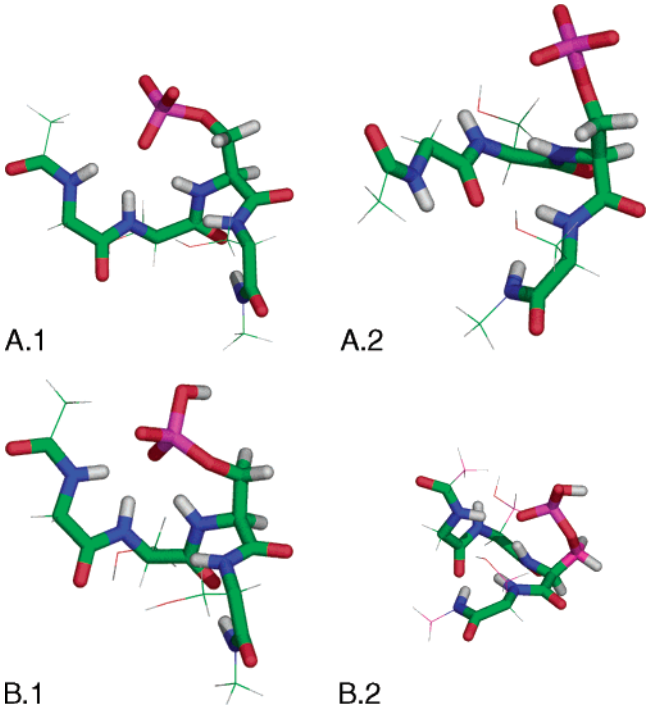

Figure 3. Representative structures from GB/SA simulation of doubly charged (A) and singly charged (B) phosphopeptides. The backbone and phosphoserine side chain is shown in sticks. A.1 and B.1 are similar conformations in which the phosphate forms multiple hydrogen bonds with backbone amide NH groups N-terminal to it. A.2 and B.2 are conformations in which the phosphate does not form internal hydrogen bonds and is well solvated.

hydrogen bond to an adjacent NH group is already present (data not shown). Thus, we find that the dynamics can be understood, to a first approximation, in terms of a cooperative transition between a state in which the phosphate group is well solvated, and one in which it forms multiple (generally 3) hydrogen bonds with amide groups N-terminal to it. This is not surprising because the entropic cost of hydrogen bonding to an adjacent amide hydrogen is effectively lowered.

Clustering of the TIP3P and GB/SA trajectories yielded two clusters. The representative structures (Figure 3a) are consistent with a cooperative transition; the representative structure of cluster 1 shows 3 hydrogen bonds between the phosphate moiety and backbone amides, whereas the representative structure for cluster 2 shows none. None of the clustering results for the GB/SA and the TIP3P simulation trajectories produced representative structures involving only 1 or 2 hydrogen bonds to backbone amides. Such intermediate states would be necessary if no cooperativity existed. The relative population between cluster 1 and cluster 2 was approximately 3:1 in the GB/SA simulation.

The other possible hydrogen bond donors on the phosphopeptide, beyond the backbone NH groups, are the hydroxyl groups on the Ser2 and Ser4 side chains. However, for both the explicit solvent and GB/SA simulations, the hydrogen bonding probability to the OH groups was less than 1%. This result is somewhat surprising, given that hydroxyl groups are almost as common hydrogen bonding partners to phosphate ions as amide hydrogens, in our survey of phosphorylated proteins in the PDB. The minor role for the hydroxyl hydrogens in our simulations may be due to the structure of this peptide. Six covalent bonds separate any of the phosphate acidic oxygens and the amide hydrogen on pSer3; the closest hydroxyl hydrogen is 10 bonds away. Thus, there is likely a higher entropic loss incurred upon forming a hydrogen bond between the phosphate ion and a hydroxyl hydrogen than the corresponding hydrogen bond with a backbone amide hydrogen. This argument also suggests that hydrogen bonds involving the phosphate and hydroxyl groups would not show cooperativity as discussed above for the amide NH groups; in fact, our data indicate that the hydrogen bonds involving the hydroxyl groups form independently. These entropy arguments, combined with the 5:2 amide to hydroxyl hydrogen ratio, provide a qualitative rationalization for the low hydrogen bonding probability to the hydroxyl groups in the GB/SA simulations.

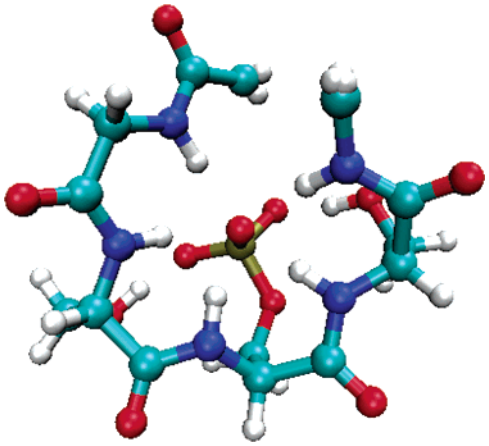

Figure 4. Snapshot from simulation of the phosphopeptide using a distance dependent dielectric ($\epsilon = r$). The phosphate groups forms hydrogen bonds with all possible hydrogen bond donors.

In contrast to the explicit solvent and GB/SA results, hydrogen bonding between the phosphate ion and hydroxyl groups is observed in the simulations using a distance dependent dielectric. The percentage is almost invariant as a function of charge and is nearly 100% for $\epsilon = r$, and 25−30% for $\epsilon = 4r$. The simulations using a $\epsilon = r$ distance dependent dielectric were typified by the conformation displayed in Figure 4. The peptide is arranged so that every possible hydrogen bond donor interacts with the phosphate group.

Comparison of Explicit Solvent Models. We have performed simulations of the −2 phosphopeptide with 3 explicit water models—TIP3P, TIP4P and SPC/E—for a single set of partial charges (those with the phosphorus charge of 1.5). We were motivated to test different explicit solvent models due to some significant differences in properties observed in simulations of pure water (e.g., ref 66) and of solvated ions (e.g., ref 30).

The calculated coupling constants are displayed in Table 3. The TIP4P and SPC/E water models generate results that are quantitatively but not qualitatively different than the TIP3P results. In particular, both TIP4P and SPC/E show less hydrogen bonding to the amide NH groups than TIP3P. These results seem reasonable on the basis of known properties of these solvent models. In particular, TIP4P water is known to be more structured than TIP3P.[36,67] A recent study[66] has also shown SPC/E water to be more structured than TIP3P. We hypothesize that a larger degree of structure around the phosphate ion increases the desolvation cost for the formation of an internal hydrogen bond.

Despite these minor differences among the results, all of the explicit solvent models evaluated here appear to be largely successful in modeling the condensed phase environment for a phosphorylated species. This is encouraging because these models lack polarizability.

Simulations of the Protonated Phosphopeptide. In addition to the doubly negative phosphopeptide, we also simulate the

TABLE 5: Effect of Phosphate Ionization State on Calculated Coupling Constants[a]

	doubly charged phosphate		singly charged phosphate	
	GB/SA	experiment	GB/SA	experiment
Gly1	4.12 (0.03)	5.63 (0.12)	3.89 (0.04)	5.66 (0.11)
Ser2	6.62 (0.11)	6.65 (0.12)	6.89 (0.34)	6.52 (0.11)
pSer3	5.73 (0.10)	5.48 (0.12)	6.69 (0.14)	6.52 (0.11)
Ser4	7.37 (0.03)	6.93 (0.12)	7.70 (0.03)	7.47 (0.11)

[a] Experimental results are listed for comparison. In parenthesis is the standard deviation of calculated results or the reported experimental error.

singly charged (−1), protonated species. Except for the extra proton and the partial charges on the phosphate group, the phosphopeptide parameters were unchanged. For computational efficiency, this system was only simulated by using the GB/SA model. To obtain atomic charges, methyl biphosphate was subjected to (1) a gas phase HF/6-31G** geometry optimization followed by (2) a single point electronic structure calculation HF/LMP2/SCRF/cc-pvtz(-f) and finally (3) electrostatic potential fitting. The partial charges for the phosphorus atom and the acidic oxygens were +1.5 and −0.98 respectively, whereas the hydroxyl oxygen and hydrogen were −0.7 and 0.5, respectively. These results seem reasonable because the phosphorus and acidic oxygen partial charges are similar to the set with a bond dipole moment of 8.75 D in Table 2. The coupling constant results are reported in Table 5, where they are compared with the experimental results at low pH. The results are in agreement with experiment to within 0.4 Hz (except for Gly1, as discussed above). Moreover, the relatively large shifts in the coupling constants for pSer3 and Ser4 between the singly and doubly charged species are quantitatively reproduced by the simulations, to within 0.2 Hz.

The shifts in the coupling constants with protonation state of the phosphate appear to be caused by quantitative but not qualitative differences in hydrogen bonding propensity. Table 6 shows that the overall P−O/N−H hydrogen bonding probability is slightly larger (up to 12% higher) for the −1 species, consistent with our expectation that a lower overall charge reduces the free energy cost of hydrogen bonding to backbone amides. Unlike the unprotonated phosphate, where all 3 acidic oxygens are equivalent, the hydrogen bonding propensities of the 3 oxygens of the protonated phosphate group are dramatically different. The protonated oxygen, which can act as either a donor or acceptor, shows little hydrogen bonding; the asymmetry in hydrogen bonding of the other two oxygens is likely due to their stereochemical difference. The unprotonated oxygens compensate for the limited hydrogen bonding of the protonated oxygen and produce a small net increase in the overall hydrogen bonding probability.

The change in overall hydrogen bonding propensity and other ensemble properties is remarkably small between the two protonation states, given the large change in the partial charges on the phosphate group. In Figure 5, we explore the strengths

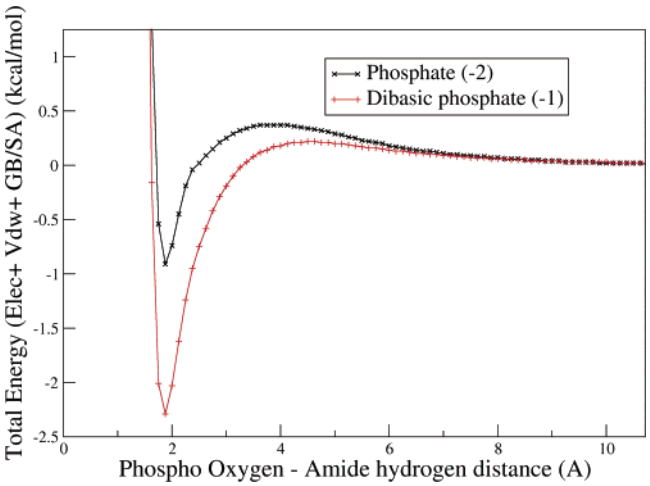

Figure 5. Energy for hydrogen bonding between the phosphate group (singly and doubly charged) and an amide NH group. Solvent effects were incorporated using GB/SA. The reaction coordinate was a direct linear approach between the P−O and N−H bond vectors. For the singly charged, protonated phosphate, the hydrogen bond was made to an unprotonated oxygen.

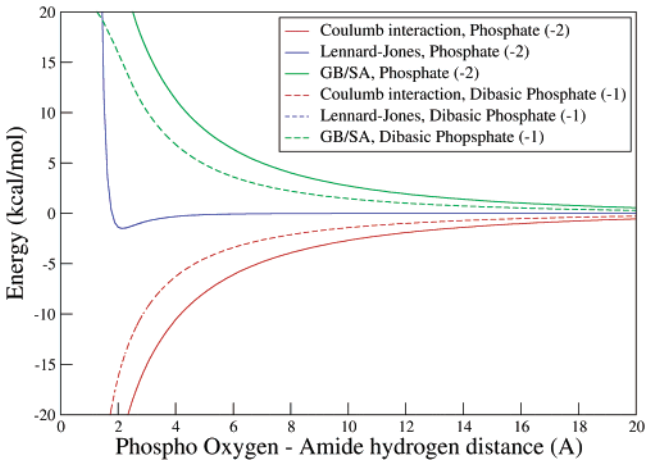

Figure 6. Energy components for the energy curves of Figure 5. Comparison of energetics in hydrogen bonding to the fully −2 phosphate (solid lines) moiety versus the −1, protonated phosphate (dashed lines). The Lennard-Jones nonbonded interactions for the phosphate group are the same in both protonation states, and thus only a single line is seen.

of the P−O/N−H hydrogen bonds in more detail by plotting the energy of interaction (force field + GB/SA) for a model system consisting of ethyl phosphate and *N*-methyl ethanamide. Specifically, we performed single point calculations for a series of conformations in which the molecules were constrained such that the P−O and H−N vectors were collinear, for both unprotonated (−2) and singly protonated (−1) phosphate. (For the −1 species, the P−O group involved in forming the hydrogen bond is unprotonated.) For both protonation states, the hydrogen bond is weakly favorable, but the singly protonated

TABLE 6: Effect of Phosphate Ionization State on Hydrogen Bonding Probability[a]

	doubly charged phosphate				singly charged phosphate			
	overall	O1	O2	O3	overall	OH	O2	O3
Gly1	56.3% (4%)	19.0% (3%)	18.5% (3%)	18.9% (4%)	57.8% (7%)	0.0% (0%)	44.0% (8%)	13.0% (5%)
Ser2	50.8% (4%)	17.0% (3%)	17.3% (3%)	16.9% (4%)	51.1% (6%)	0.0% (0%)	40.0% (7%)	11.1% (4%)
pSer3	60.4% (4%)	20.3% (3%)	19.9% (3%)	20.7% (4%)	72.2% (8%)	18.2% (1%)	47.2% (8%)	14.2% (5%)
Ser4	7.8% (2%)	2.3% (0.6%)	1.6% (0.5%)	3.8% (1%)	17.1% (4%)	3.1% (0.6%)	15.8% (4%)	4.0% (0.2%)

[a] The hydrogen bonding probabilities were computed for each phosphate oxygen. In the case of the singly charged phosphate, the hydroxyl oxygen is labeled OH. All calculations are performed using GB/SA solvent. The standard error of the mean is in parenthesis.

phosphate has a somewhat (~2 *kT*) deeper well. The individual components of the energy are plotted in Figure 6. The stronger electrostatic interaction of the −2 species is slightly exceeded by the larger desolvation penalty yielding the small overall energy difference.

The ensemble of structures for the singly charged phosphopeptide, like the doubly charged phosphopeptide, shows an equilibrium between two states (no hydrogen bonds and multiple backbone hydrogen bonds), as shown in Figure 3. The representative structures from the two clusters are very similar for the two charge states. As in the case of the doubly charged phosphopeptide, only 2 clusters were found.

Conclusion

In this work we have simulated a capped phosphorylated peptide, Ace-Gly-Ser-pSer-Ser-Nme, by a variety of solvent models, and compared the results to each other and to experimental observables from an NMR experiment. The major conclusions are

1. The quality of agreement to experiment depends sensitively on both the choice of partial charges for the phosphorylated side chain and the solvent model. Partial charges of +1.45 to +1.50 for the P, −0.99 to −1.05 for the acidic oxygens, and approximately −0.66 for the ester oxygen give the best agreement with experiment using explicit solvent and Generalized Born implicit solvent. However, the "optimal" partial charges are slightly different for each solvent model.

2. The explicit solvent models (TIP3P, TIP4P, SPC/E) and a Generalized Born implicit solvent model (GB/SA[35]) both gave good agreement with experiment given appropriate partial charges. The apparently good performance of the GB/SA solvent model is encouraging, because it provides a much more efficient means of simulating phosphorylated proteins than the explicit solvent models. Nonetheless, we do not wish to overstate the significance of this result; more work is clearly needed. First, in simulations on the unphosphorylated Gly-Ser-Ser-Ser peptide, we have found that explicit solvent simulations give significantly better agreement with experiment than GB/SA (results in Supporting Information). Second, in other work, one of us (MPJ) has elucidated specific deficiencies of implicit solvent models related to the inability to represent first-shell solvation effects,[27] and these same deficiencies likely apply to phosphorylated residues as well. In particular, implicit solvent does not reproduce "solvent-separated minima" in the potentials of mean force for ion pairs and hydrogen bonds.[28] This effect is observed in this study as well (Figure S2) but apparently does not strongly perturb the ensemble averages of the backbone torsion angles measured by experiment.

3. Distance dependent dielectric solvent models were unable to properly simulate the condensed phase environment for the phosphorylated peptide, over the range of partial charges tested here, due to gross overstabilization of hydrogen bonds involving the phosphate group.

4. We observed a strong correlation between the calculated NMR coupling constants and the propensity to form hydrogen bonds between the phosphate group and backbone amide NH groups. This is reasonable, because hydrogen bonding imposes a restraint on the molecule that it would otherwise not have. To a reasonable approximation, the simulations with explicit solvent and GB/SA show transitions between two states of the phosphopeptide: one in which the phosphate forms no hydrogen bonds to the peptide and is thus fully solvated, and one in which it forms multiple hydrogen bonds to NH groups, especially the NH group on the phosphorylated residue itself and the residues N-terminal to it. Hydrogen bonds to the OH groups on the Ser side chains appear to be unimportant in these simulations.

5. The strengths of hydrogen bonds involving the phosphate group involve a subtle tradeoff between the direct Coulomb's law electrostatic attraction and the free energy cost of partially desolvating the phosphate group. Although this conclusion is not new or unique to this study, this tradeoff is particularly striking in the case of the phosphate group with the −2 charge. The inability of the distance dependent dielectric simulations to reproduce the experimental results is simply due to the lack of any treatment of desolvation. The strengths of the P−O/N−H hydrogen bonds decrease with increasing dipole on the P−O bond, because the desolvation penalty increases more rapidly than the favorable dipole/dipole interaction.

6. The ensemble averages obtained for the phosphopeptide in the −1 (singly protonated phosphate) and −2 (fully deprotonated phosphate) charge states are surprisingly similar. The results with the singly protonated phosphate show slightly higher propensities for hydrogen bonding to the backbone amide NH groups. When the charge on the phosphate is increased from −1 to −2, the strength of the electrostatic attraction of course increases significantly, but this effect is very nearly canceled by the increase in the free energy cost of desolvation upon forming a hydrogen bond. This interpretation is slightly complicated by the fact that the protonated oxygen on the −1 phosphate can act as either a donor or acceptor.

In this work, we have examined only a subset of intriguing questions regarding solvation of phosphorylated residues. In ongoing work, we are performing additional explicit solvent simulations to study in more detail the solvent structures around the phosphate group in solution and when it forms hydrogen bonds, the possible role of dielectric saturation,[68] and the role of solvent polarizability; these results will be reported elsewhere.

Acknowledgment. We thank John Chodera and Kevin Masukawa (UCSF) and members of the Jacobson group for helpful conversations. This work was supported by NSF grants MCB-0302445 and MCB-0346399. S.E.W. acknowledges support from Burroughs-Wellcome through a UCSF Program in Quantitative Biology fellowship. K.B. acknowledges support from an NSF Postdoctoral Fellowship in Interdisciplinary Informatics. M.P.J. is a consultant to Schrödinger, Inc.

Supporting Information Available: Figures of (1) backbone dihedral angle as a function of simulation time, (2) probability of finding the phosphate oxygens at a given distance from the NH group on Ser2, and (3) backbone J-coupling results for the unphosphorylated GSSS peptide. This material is available free of charge via the Internet at http://pubs.acs.org.

References and Notes

(1) Audette, G. F.; Engelmann, R.; Hengstenberg, W.; Deutscher, J.; Hayakawa, K.; Quail, J. W.; Delbaere, L. T. *J. Mol. Biol.* **2000**, *303*, 545.

(2) Chen, Z.; Gibson, T. B.; Robinson, F.; Silvestro, L.; Pearson, G.; Xu, B.; Wright, A.; Vanderbilt, C.; Cobb, M. H. *Chem. Rev.* **2001**, *101*, 2449.

(3) Patel, A. J.; Honore, E. *Trends Neurosci.* **2001**, *24*, 339.

(4) Martens, J. R.; Kwak, Y. G.; Tamkun, M. M. *Trends Cardiovasc. Med.* **1999**, *9*, 253.

(5) Vermeulen, K.; Van Bockstaele, D. R.; Berneman, Z. N. *Cell Prolif.* **2003**, *36*, 131.

(6) Feng, M. H.; Philippopoulos, M.; MacKerell, A. D.; Lim, C. *J. Am. Chem. Soc.* **1996**, *118*, 11265.

(7) Johnson, L. N.; Lewis, R. J. *Chem. Rev.* **2001**, *101*, 2209.

(8) Johnson, L. N.; O'Reilly, M. *Curr. Opin. Struct. Biol.* **1996**, *6*, 762.

(9) Stultz, C. M.; Levin, A. D.; Edelman, E. R. *J. Biol. Chem.* **2002**, *277*, 47653.

(10) Roche, P.; Mouawad, L.; Perahia, D.; Samama, J. P.; Kahn, D. *Protein Sci.* **2002**, *11*, 2622.
(11) Peters, G. H.; Frimurer, T. M.; Andersen, J. N.; Olsen, O. H. *Biophys. J.* **2000**, *78*, 2191.
(12) Schneider, M. L.; Post, C. B. *Biochemistry* **1995**, *34*, 16574.
(13) Wozniak-Celmer, E.; Oldziej, S.; Ciarkowski, J. *Acta Biochim. Polonica* **2001**, *48*, 35.
(14) Tomoo, K.; Shen, X.; Okabe, K.; Nozoe, Y.; Fukuhara, S.; Morino, S.; Sasaki, M.; Taniguchi, T.; Miyagawa, H.; Kitamura, K.; Miura, K.; Ishida, T. *J. Mol. Biol.* **2003**, *328*, 365.
(15) Young, M. A.; Gonfloni, S.; Superti-Furga, G.; Roux, B.; Kuriyan, J. *Cell* **2001**, *105*, 115.
(16) Phan-Chan-Du, A.; Hemmerlin, C.; Krikorian, D.; Sakarellos-Daitsiotis, M.; Tsikaris, V.; Sakarellos, C.; Marinou, M.; Thureau, A.; Cung, M. T.; Tzartos, S. J. *Biochemistry* **2003**, *42*, 7371.
(17) Fu, Z.; Aronoff-Spencer, E.; Backer, J. M.; Gerfen, G. J. *Proc. Natil. Acad. Sci. U.S.A.* **2003**, *100*, 3275.
(18) Bartova, I.; Otyepka, M.; Kriz, Z.; Koca, J. *Protein Sci* **2004**, *13*, 1449.
(19) Kubala, M.; Obsil, T.; Obsilova, V.; Lansky, Z.; Amler, E. *Physiol. Res.* **2004**, *53 Suppl 1*, S187.
(20) Mendieta, J.; Gago, F. *J. Mol. Graph. Model* **2004**, *23*, 189.
(21) Miranda, F. F.; Thorolfsson, M.; Teigen, K.; Sanchez-Ruiz, J. M.; Martinez, A. *Protein Sci*. **2004**, *13*, 1219.
(22) Obsilova, V.; Herman, P.; Vecer, J.; Sulc, M.; Teisinger, J.; Obsil, T. *J. Biol. Chem.* **2004**, *279*, 4531.
(23) Suenaga, A.; Kiyatkin, A. B.; Hatakeyama, M.; Futatsugi, N.; Okimoto, N.; Hirano, Y.; Narumi, T.; Kawai, A.; Susukita, R.; Koishi, T.; Furusawa, H.; Yasuoka, K.; Takada, N.; Ohno, Y.; Taiji, M.; Ebisuzaki, T.; Hoek, J. B.; Konagaya, A.; Kholodenko, B. N. *J. Biol. Chem.* **2004**, *279*, 4657.
(24) Smart, J. L.; McCammon, J. A. *Biopolymers* **1999**, *49*, 225.
(25) Kosinsky, Y. A.; Volynsky, P. E.; Lagant, P.; Vergoten, G.; Suzuki, E.; Arseniev, A. S.; Efremov, R. G. *J. Comput. Chem.* **2004**, *25*, 1313.
(26) Shen, T. Y.; Wong, C. F.; McCammon, J. A. *J. Am. Chem. Soc.* **2001**, *123*, 9107.
(27) Yu, Z.; Jacobson, M. P.; Rapp, C. S.; Friesner, R. A. *J. Phys. Chem. B* **2004**, *108*, 6643.
(28) Masunov, A.; Lazaridis, T. *J. Ame. Chem. Soc.* **2003**, *125*, 1722.
(29) Alper, H. E.; Levy, R. M. *J. Phys. Chem.* **1990**, *94*, 8401.
(30) Soetens, J. C.; Millot, C.; Chipot, C.; Jansen, G.; Angyan, J. G.; Maigret, B. *J. Phys. Chem. B* **1997**, *101*, 10910.
(31) Xu, H. F.; Stern, H. A.; Berne, B. J. *J. Phys. Chem. B* **2002**, *106*, 2054.
(32) Beveridge, D. L.; McConnell, K. J. *Curr. Opin. Struct. Biol.* **2000**, *10*, 182.
(33) Norberg, J.; Nilsson, L. *Acc. Chem. Res.* **2002**, *35*, 465.
(34) Arthanari, H.; McConnell, K. J.; Beger, R.; Young, M. A.; Beveridge, D. L.; Bolton, P. H. *Biopolymers* **2003**, *68*, 3.
(35) Tsui, V.; Case, D. A. *J. Am. Chem. Soc.* **2000**, *122*, 2489.
(36) Jorgensen, W. L.; Chandrasekhar, J.; Madura, J. D.; Impey, R. W.; Klein, M. L. *J. Chem. Phys.* **1983**, *79*, 926.
(37) Berendsen, H. J. C.; Grigera, J. R.; Straatsma, T. P. *J. Phys. Chem.* **1987**, *91*, 6269.
(38) Dominy, B. N.; Brooks, C. L. *J. Phys. Chem. B* **1999**, *103*, 3765.
(39) Tsui, V.; Case, D. A. *Biopolymers* **2000**, *56*, 275.
(40) Tholey, A.; Lindemann, A.; Kinzel, V.; Reed, J. *Biophys. J.* **1999**, *76*, 76.
(41) Berman, H. M.; Westbrook, J.; Feng, Z.; Gilliland, G.; Bhat, T. N.; Weissig, H.; Shindyalov, I. N.; Bourne, P. E. *Nucl. Acids Res.* **2000**, *28*, 235.
(42) Case, D. A.; D. A. P., Caldwell, J. W.; Cheatham, T. E., III; Wang, J.; Ross, W. S.; Simmerling, C. L.; Darden, T. A.; Merz, K. M.; Stanton, R. V.; Cheng, A. L.; Vincent, J. J.; Crowley, M.; Tsui, V.; Gohlke, H.; Radmer, R. J.; Duan, Y.; Pitera, J.; Massova, I.; Seibel, G. L.; Singh, U. C.; Weiner, P. K.; Kollman, P. A. AMBER 7; University of California: San Francisco, CA, 2002.
(43) Okur, A.; Strockbine, B.; Hornak, V.; Simmerling, C. *J. Comput. Chem.* **2003**, *24*, 21.
(44) Berendsen, H. J. C.; Postma, J. P. M.; Vangunsteren, W. F.; Dinola, A.; Haak, J. R. *J. Chem. Phys.* **1984**, *81*, 3684.
(45) Toukmaji, A.; Sagui, C.; Board, J.; Darden, T. *J. Chem. Phys.* **2000**, *113*, 10913.
(46) Essmann, U.; Perera, L.; Berkowitz, M. L.; Darden, T.; Lee, H.; Pedersen, L. G. *J. Chem. Phys.* **1995**, *103*, 8577.
(47) Darden, T.; York, D.; Pedersen, L. *J. Chem. Phys.* **1993**, *98*, 10089.
(48) J.-P. Ryckart, G. C. H. J. C. B. *J. Comput. Phys.* **1977**, *23*, 327.
(49) Mitsutake, A.; Sugita, Y.; Okamoto, Y. *J. Chem. Phys.* **2003**, *118*, 6664.
(50) Mitsutake, A.; Sugita, Y.; Okamoto, Y. *J. Chem. Phys.* **2003**, *118*, 6676.
(51) Sugita, Y.; Okamoto, Y. *Chem. Phys. Lett.* **1999**, *314*, 141.
(52) Janke, W. Statistical Analysis of Simulations: Data Correlation and Error Estimation. In *Quantum Simulations of Complex Many-Body Systems: From Theory to Algorithms, Lecture Notes*; Grotendorst, J., M. D., Muramatsu, A., Ed.; John von Neumann Institute for Computing: Julich, 2002; Vol. 10, p 423.
(53) Jaguar 5.0, S., L. L. C. Jaguar; 5.0 ed. Portland, OR, 1991−2003.
(54) Marten, B.; Kim, K.; Cortis, C.; Friesner, R. A.; Murphy, R. B.; Ringnalda, M. N.; Sitkoff, D.; Honig, B. *J. Phys. Chem.* **1996**, *100*, 11775.
(55) Tannor, D. J.; Marten, B.; Murphy, R.; Friesner, R. A.; Sitkoff, D.; Nicholls, A.; Ringnalda, M.; Goddard, W. A.; Honig, B. *J. Am. Chem. Soc.* **1994**, *116*, 11875.
(56) Karplus, M. *J. Phys. Chem.* **1959**, *30*, 11.
(57) Vuister, G. W.; Bax, A. *J. Am. Chem. Soc.* **1993**, *115*, 7772.
(58) Michael Feig, J. K., Charles L. Brooks, III. MMTB Tool Set. In *MMTSB NIH Research Resource* The Scripps Research Institute, 2001.
(59) Xu, S.; Kamath, M. V.; Capson, D. W. *Pattern Recognition Lett.* **1993**, *14*, 7.
(60) Cieplak, P.; Cornell, W. D.; Bayly, C.; Kollman, P. A. *J. Comput. Chem.* **1995**, *16*, 1357.
(61) Chirlian, L. E.; Francl, M. M. *J. Comput. Chem.* **1987**, *8*, 894.
(62) Woods, R. J.; Khalil, M.; Pell, W.; Moffat, S. H.; Smith, V. H. *J. Comput. Chem.* **1990**, *11*, 297.
(63) Saebo, S.; Pulay, P. *Annu. Rev. Phys. Chem.* **1993**, *44*, 213.
(64) Jorgensen, W. L.; Tiradorives, J. *J. Am. Chem. Soc.* **1988**, *110*, 1666.
(65) Humphrey, W.; Dalke, A.; Schulten, K. *J. Mol. Graph.* **1996**, *14*, 33.
(66) Mark, P.; Nilsson, L. *J. Phys. Chem. A* **2001**, *105*, 9954.
(67) Guillot, B. *J. Mol. Liq.* **2002**, *101*, 219.
(68) Jayaram, B.; Fine, R.; Sharp, K.; Honig, B. *J. Phys. Chem.* **1989**, *93*, 4320.